Applied Physics A (2022) 128:626
https://doi.org/10.1007/s00339-022-05758-9

**Applied Physics A**
**Materials Science & Processing**

# A simple strategy towards construction of fluorine-free superhydrophobic aluminum alloy surfaces: self-cleaning, anti-corrosion and anti-frost

**Wenyan Li[1] · Hanming Yang[2] · Sen Xue[1] · Tao Shi[1] · Qiang Wang[1] · Huaqiao Peng[1]**

Received: 24 November 2021 / Accepted: 7 June 2022 / Published online: 30 June 2022


**Abstract**
This work introduced a simple method to fabricate a superhydrophobic aluminum alloy surface based on a combination strategy of chemical etching using $HCl/H_2O_2$ mixture and modification by polydimethylsiloxane (PDMS). The chemical composition, morphology and hydrophobicity of the surface were characterized by FTIR, EDS, 3D optical profiler, SEM and contact angle system. The results show that the fabricated micro/nano-scale hierarchical structures after being modified with PDMS can results in a good anti-adhesion and resistance to wettability with a water contact angle as high as 161° and a sliding angle of 7°. Also, the superhydrophobic surface displayed excellent thermal stability and self-cleaning performance. Furthermore, electrochemical tests indicated that the superhydrophobic surface was endowed with good corrosion resistance property. The prepared surface was demonstrated to have a commendable resistance to corrosion, exhibiting a lower corrosion current density of $2.5 \times 10^{-9}$ A/cm$^2$ and a higher corrosion potential of − 0.58 V. Compared to original aluminum alloy plate, the superhydrophobic surface had an ability to delay icing with the obviously decreased frosting area. To a certain extent, these investigations opened up possibilities for applications of superhydrophobic surface, especially in the fields of self-cleaning, anti-corrosion and anti-frost.

**Keywords** Chemical etching · Aluminum alloy · PDMS · Superhydrophobicity · Self-cleaning · Anti-corrosion · Anti-frost

## 1 Introduction

Superhydrophobic surfaces with a water contact angle (CA) higher than 150° and a sliding angle (SA) lower than 10° have a broad potential application in daily life and industrial production, such as anti-fogging of glass surface, self-cleaning of traffic lights, drag reduction, anti-fouling, selective absorption of textiles, etc. [1–5]. The preparation of a superhydrophobic surface mainly depends on the combination of the surface hierarchical microstructure and the low-surface energy materials. Traditionally, common superhydrophobic surface are prepared by various methods include chemical etching [6–8], sol–gel [9, 10], chemical deposition [11] and anodic oxidation [12, 13]. Yang et al. [14] fabricated a superhydrophobic surface on AA3003 with a structure consisting of microrods and nanosheets via a chemical etching approach combined with modification by stearic acid alcohol solution. Lu et al. [15] reported a simple and inexpensive electrochemical method for preparing robust superhydrophobic titanium surfaces. They all successfully prepared superhydrophobic surfaces, which were characterized by a series methods. However, stearic alcohol and fluoroalkylsilane (FAS) they used are slightly toxic or environmentally unfriendly.

In recent years, polydimethylsiloxane (PDMS) has been widely used in the preparation of superhydrophobic surfaces due to its chemical inertness, thermal stability, biocompatibility [16–20], optical property and hydrophobicity [21]. Different from the expensive fluoroalkylsilane used in the fabrication of superhydrophobic surfaces, PDMS is fluorine-free, environment-friendly, cheap and easy to obtain.

✉ Tao Shi
shitao@fccc.org.cn

✉ Huaqiao Peng
penghuaqiao@fccc.org.cn

[1] The Second Research Institute of Civil Aviation Administration of China, Chengdu 610041, People's Republic of China

[2] Faculty of Geosciences and Environmental Engineering, Southwest Jiaotong University, Chengdu 610031, People's Republic of China

Moreover, PDMS can be dissolved in organic solvents easily and then superhydrophobic composite with the advantages of inorganic and organic materials can be obtained by the combination of PDMS and inorganic particles [22]. Aleksander Cholewinski et al. [23] fabricated a robust superhydrophobic bilayer coating with a facile dip-coating process containing polydimethylsiloxane (PDMS)-functionalized silica particles on top and an epoxy bonding layer at the base. Sun et al. [24] prepared the superhydrophobic organic–inorganic composite coatings by nano-$TiO_2$ and PDMS with the water contact angle of 170°. Their organic–inorganic blending method is simple and it does not need special equipment, which could be used to prepare large-area superhydrophobic coating. However, expensive inorganic nanoparticles were added in their coatings, which may cause adverse effects on human health.

In this paper, the superhydrophobic surface is conveniently prepared by chemical etching and dip coating. The aluminum alloy plate is totally immersed into $HCl/H_2O_2$ mixture to obtain micro–nano-structure, then passivated by PDMS layer to fabricate superhydrophobic surface, which has the characteristics of simple, reliable, low cost and fast reaction. Moreover, the prepared surface also demonstrates excellent self-cleaning, anti-corrosion and anti-frost properties. This superhydrophobic surface is believed to have wide industrial application prospects potentially.

## 2 Experimental section

### 2.1 Materials

SAE AMS 4037 aluminum alloy plates were provided by Kaiser Aluminum Corporation, USA, and cut into 50 mm × 25 mm × 2 mm pieces. Grit 1200 sand paper was purchased from Buehler, USA. Polydimethylsiloxane (PDMS) was obtained from Dow Corning Corporation. Hydrogen peroxide ($H_2O_2$, *w*/*w*, 30%), hydrochloric acid (HCl, *w*/*w*, 37%), ethanol, acetone and petroleum ether were purchased from Chengdu Kelong Chemical Company. All chemicals without further purification are analytical grade.

### 2.2 Preparation of the superhydrophobic surface

Aluminum alloy plate was polished by sand paper, cleaned ultrasonically in deionized water, acetone, ethanol (each for 10 min) respectively, and followed by drying in an oven. Then the plate was chemical etched at room temperature for 15 min by the mixture of hydrochloric acid (HCl, 1 mol/L) and hydrogen peroxide ($H_2O_2$, 1 mol/L). The etched plate was cleaned ultrasonically in deionized water, followed by immersion in hot water (50 °C) for 1 h, and then drying at room temperature. Finally, the etched plates were treated at 60 °C for 3 h by mixture of PDMS (0.2 g), curing agent (0.02 g) and petroleum ether with different volume, such as 5 ml, 10 ml, 20 ml, 30 ml and 40 ml, subsequently dried in an oven at 120 °C for 3 h. The prepared sample was designated as treated-Al-X, and X was represented the volume of petroleum ether.

### 2.3 Characterization

Static water contact angle (CA) and sliding angle (SA) were obtained by a contact angle system (DSA30, Kruss GmbH, Germany) at room temperature. CA values were measured by employing 3 μL of water droplets, and SA values were recorded by dosing 10 μL of water droplets under continuous tilt angular velocity of 1.5°/s. FTIR spectra was recorded in a range of 400–4000 $cm^{-1}$ with a resolution of 4 $cm^{-1}$ on an infrared spectrometer (Nicolet iS50, USA). The surface morphology and element composition of these samples were studied using a scanning electron microscope (SEM, JEOL JSM-6480LV, Japan) coupled with an energy dispersive X-ray spectrometer (EDS). The root mean square roughness (Rq) of the surfaces were measured by 3D optical profiler. For the temperature stability, CA and SA of samples modified with PDMS were measured at room temperature after continuously heating or freezing the samples for 2 h. For the chemical stability evaluation, as-prepared samples were soaked in the solution of 3.5 wt% NaCl at ambient temperature for different hours. The dynamic behaviors of water droplet on the superhydrophobic surface was conducted using a high-speed video camera (5F01M, Fuhuang Agile Device, China) with a frame rate of 1000 fps. Electrochemical corrosion test was carried out in a three-electrode cell. Measurements were performed in 3.5 wt% NaCl solution by an electrochemical workstation (PARSTAT 4000A, Princeton) at room temperature. Icing experiment was performed in a laboratory-made low-temperature cabinet, and the samples were fixed on the platform inclined at 10° from the horizontal plane. The water droplets with a diameter of 20 μm were sprayed on the sample, and the related sample appearances were recorded, respectively.

## 3 Results and discussion

### 3.1 Characterization of the superhydrophobic surface

The wettability of the original aluminum alloy surface and the etched aluminum alloy surfaces treated with varying concentrations of PDMS is shown in Table 1. It shows that the hydrophobicity of modified surfaces enhances markedly with the decrease in the concentration of PDMS. The CA

**Table 1** CA and SA of prepared samples

| Sample | The volume of petroleum ether (ml) | CA (°) | SA (°) |
|---|---|---|---|
| Al | – | 88.3 ± 1.3 | > 30 |
| etched-Al | – | 0 | – |
| treated-Al-5 | 5 | 150.2 ± 1.0 | > 30 |
| treated-Al-10 | 10 | 158.5 ± 0.8 | 8.8 ± 1.3 |
| treated-Al-20 | 20 | 158.4 ± 1.8 | 8.7 ± 0.7 |
| treated-Al-30 | 30 | 158.6 ± 0.9 | 7.5 ± 0.9 |
| treated-Al-40 | 40 | 161.1 ± 0.7 | 6.7 ± 0.2 |
| treated-Al-50 | 50 | 162.7 ± 1.1 | 7.2 ± 1.0 |
| treated-Al-60 | 60 | 161.8 ± 0.8 | 12.3 ± 0.6 |

increases to 161.1 ± 0.7° and reaches its minimum value of 6.7 ± 0.2° when the volume of petroleum ether is 40 ml.

Figure 1 shows the FTIR spectra of treated-Al-40. The broad band at 3437 $cm^{-1}$ is attributed to O–H stretching vibration, and it should correspond to remaining hydroxyl groups of prepared sample surfaces [21, 22]. The peaks at 2960 $cm^{-1}$, 2930 $cm^{-1}$ and 2850 $cm^{-1}$ are due to the C–H asymmetric and symmetric stretching of $–CH_3$ and $–CH_2–$ groups. The peak at 1631 $cm^{-1}$ is attribute to the C = O group, which might be resulted from the curing agent. The peaks appearing at 1264 $cm^{-1}$ can be assigned to the bending vibration of $Si–CH_3$. The characteristic absorption of 1098 $cm^{-1}$ and 1070 $cm^{-1}$ are assigned to the symmetric and asymmetric band stretching of Si–O–Si, respectively [23, 24]. The peak at 802 $cm^{-1}$ may relate to the rocking vibration of $Si\text{-}CH_3$. They are all characteristic peaks of PDMS.

Figure 2 reveals the surface morphology of Al, etched-Al and treated-Al-40. The original aluminum alloy exhibits a relatively flat surface combing with some scratch defects in a fixed direction. Obviously, a number of etching pits with terrace-like structure consisting of nano-scale flakes exist on aluminum alloy substrates after immersed in HCl/$H_2O_2$ mixture. The uneven and rough surface with multifarious protrusions and grooves consisting of multilayer is also observed on treated-Al-40, illustrating that the micro/nano-scale structure keeps uncharged. All these results manifest that the resultant superhydrophobic aluminum alloy surface is composed of hierarchical structure. As seen from Fig. 3, compared with the original surface, the EDS spectrum of etched surface and treated-Al-40 contains with O element with higher content besides the inherent compositions of Al and C, which implies the existence of oxidized layer on the surface after chemical etching. At the same time, Al reacts with hot water to form hydrous aluminum ($Al_2O_3{\cdot}xH_2O$), which also leads to an increase in oxygen content. And the oxide layer partially reacted with HCl and further changed into $AlCl_3$. In addition, Al is a kind of active metals, thus easily reacted with HCl and turned into $AlCl_3$. These reactions are shown as follows

$$2Al + 3H_2O_2 \rightarrow Al_2O_3 + 3H2O, \quad (1)$$

$$Al_2O_3 + 6HCl \rightarrow 2AlCl_3 + 3H_2O, \quad (2)$$

$$2Al + 6HCl \rightarrow 2AlCl_3 + 3H_2 \uparrow, \quad (3)$$

$$4Al + 3H_2O_2 + 12HCl \rightarrow 4AlCl_3 + 6H_2O + 3H_2 \uparrow. \quad (4)$$

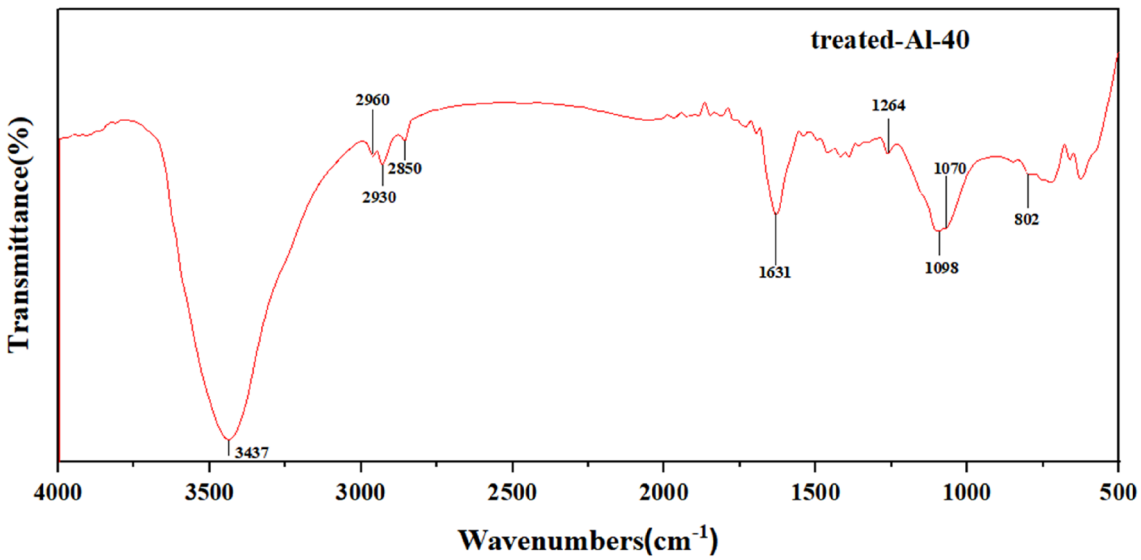


**Fig. 1** FTIR spectra of treated-Al-40

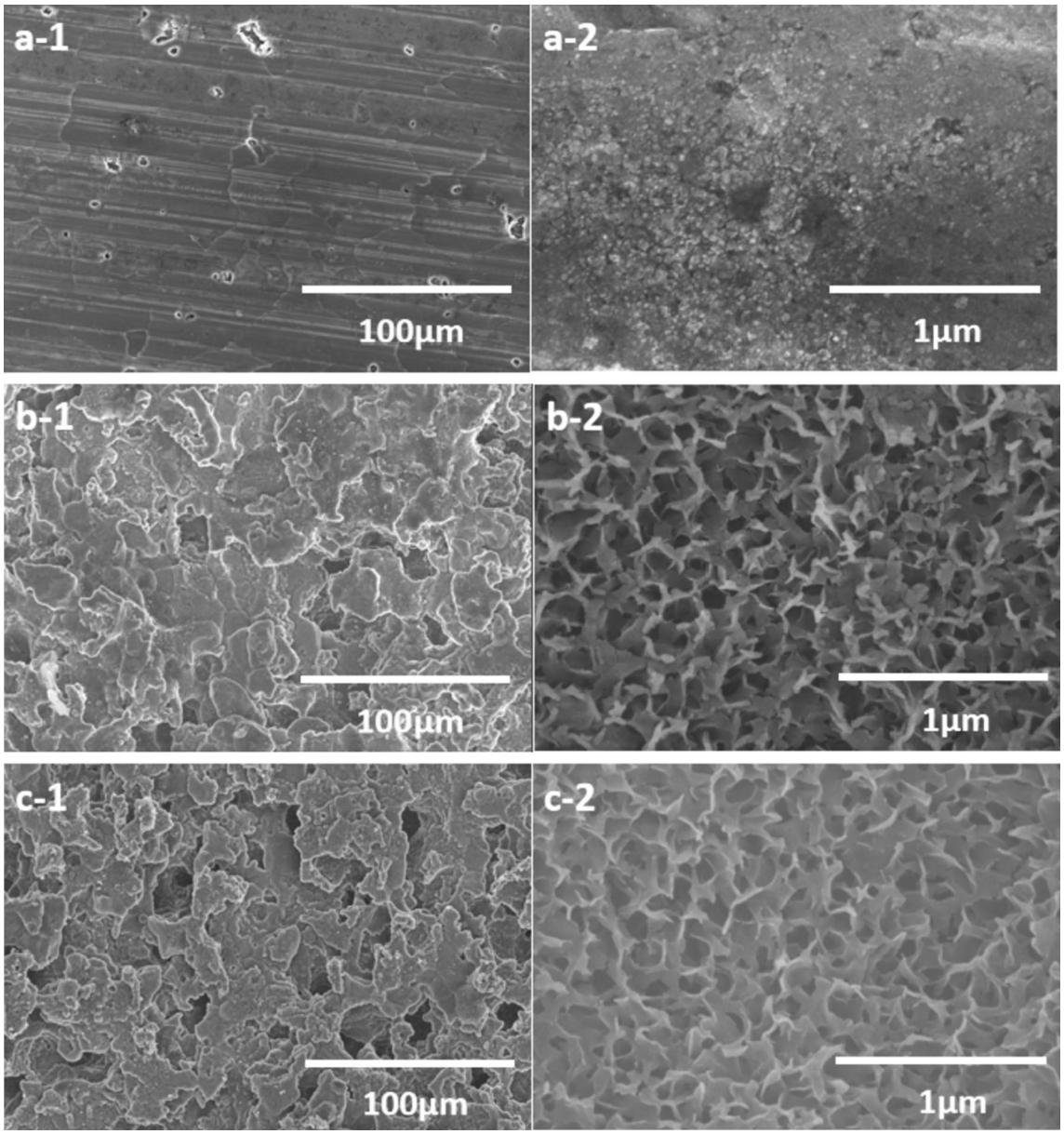


**Fig. 2** SEM images of Al (**a**), etched Al (**b**) and treated-Al-40 (**c**)

To sum up, various reactions on aluminum alloy surface result in a uniform multi-scale hierarchical structure. It is noted that a new element Si is also found on the etched aluminum plate treated by PDMS. This element is mainly derived from PDMS, indicating that PDMS film formed and covered the rough structure.

The root mean square roughness (Rq) of the surfaces is measured by 3D optical profiler, and the corresponding images are shown in Fig. 4. Aluminum alloy plate has a highly smooth surface with the Rq of $0.18 \pm 0.02$ μm. Compared to the original surface, etched-Al and treated-Al-40 both exhibit relatively high value Rq of $10.46 \pm 0.34$ μm and $7.91 \pm 0.26$ μm, respectively. The similar crisscross valleys and gullies are observed on the surfaces of etched-Al and treated-Al-40, which is quite different with the original surface. These results are consistent with SEM observation, indicating that the roughness of microstructure is one of the key factors for preparation of superhydrophobic surface.

The apparent contact angle $\theta^*$ for a water droplet in the treated-Al can be described by Cassie and Baxter equation [25] as

$$\cos\theta^* = f_1 \cos\theta - f_2, \tag{5}$$

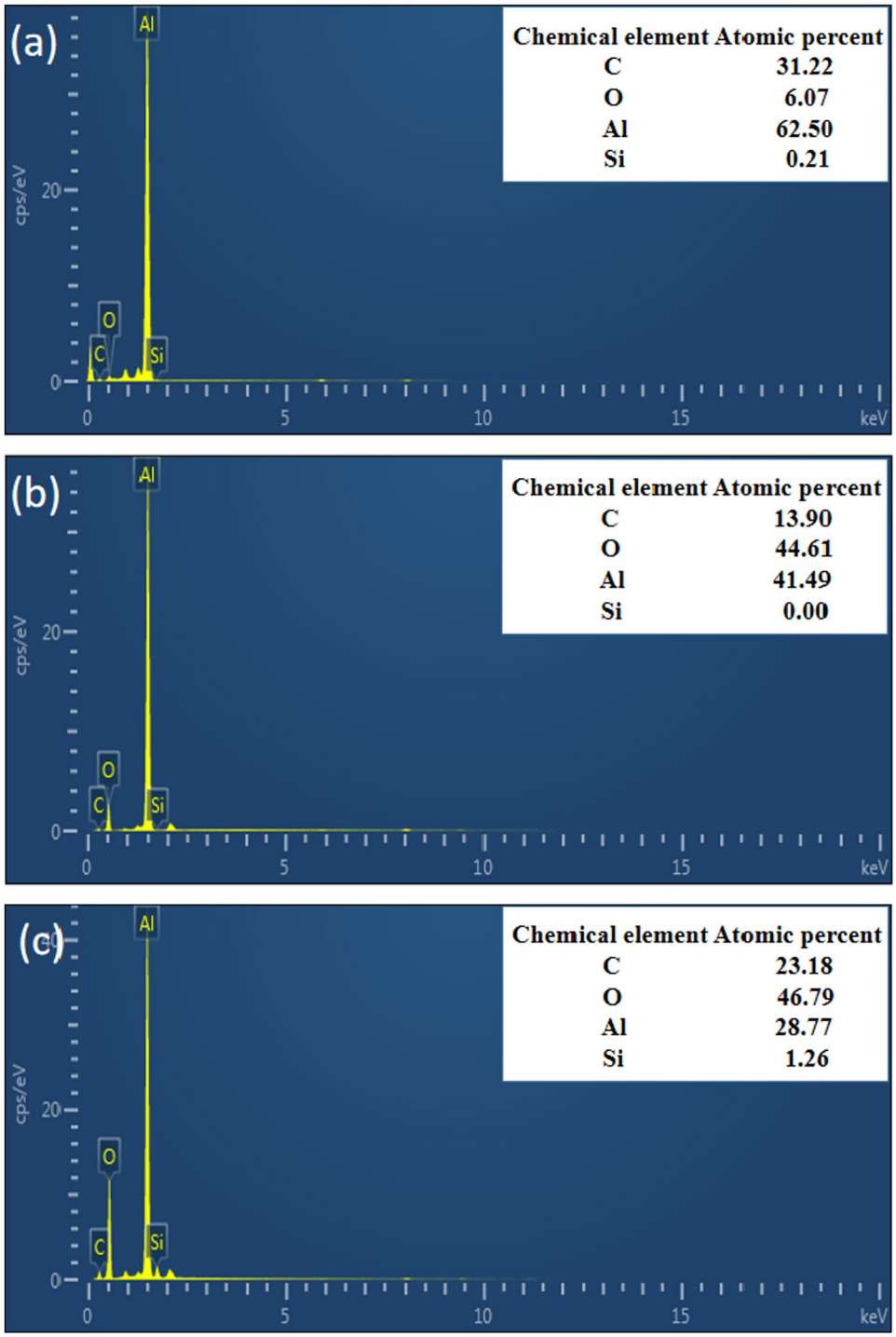


**Fig. 3** EDS spectrum of Al (**a**), etched-Al (**b**) and treated-Al-40 (**c**)

where $\theta^*$ and $\theta$ represent the contact angles of rough and smooth surfaces, respectively, $f_1$ and $f_2$ represent the area fraction of the solid surface and the contact area between the air and the droplet, respectively, and $f_1 + f_2 = 1$. As the solid–liquid contact area ($f_1$) decreases, the contact angle of rough surfaces increases, thus the hydrophobicity of the coating is improved. As shown in Fig. 5, PDMS with low surface energy covers the rough structure, and air bubbles existing between the liquid and solid groove form an air cushion, thus effectively reducing the contact area between water droplets and the surface.

### 3.2 Stability of the superhydrophobic surface

It is very important for superhydrophobic materials to remain wettability for a period of time after treatment.

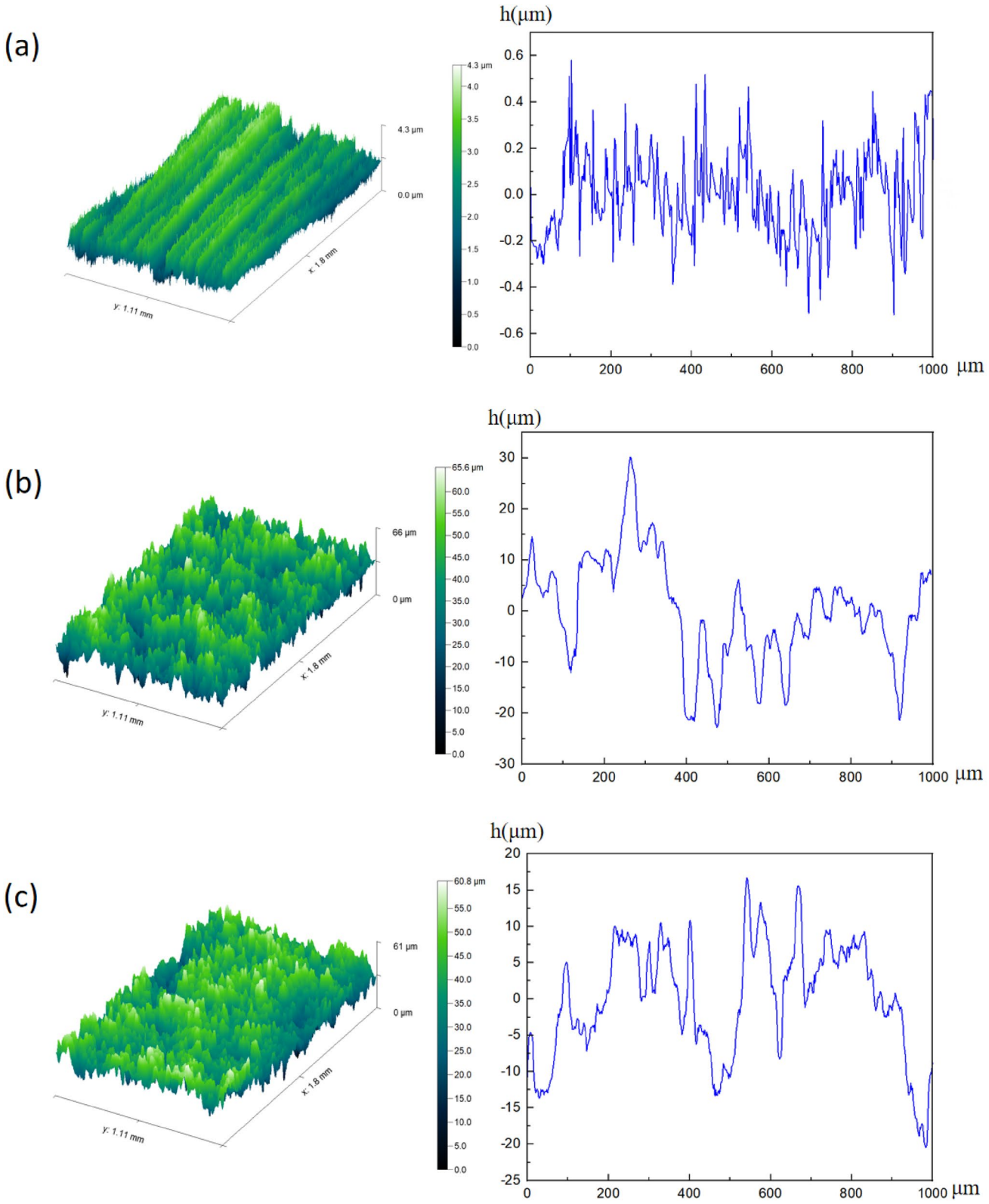


**Fig. 4** 3D images (left) and height curves (right) of Al (**a**), etched-Al (**b**) and treated-Al-40 (**c**)

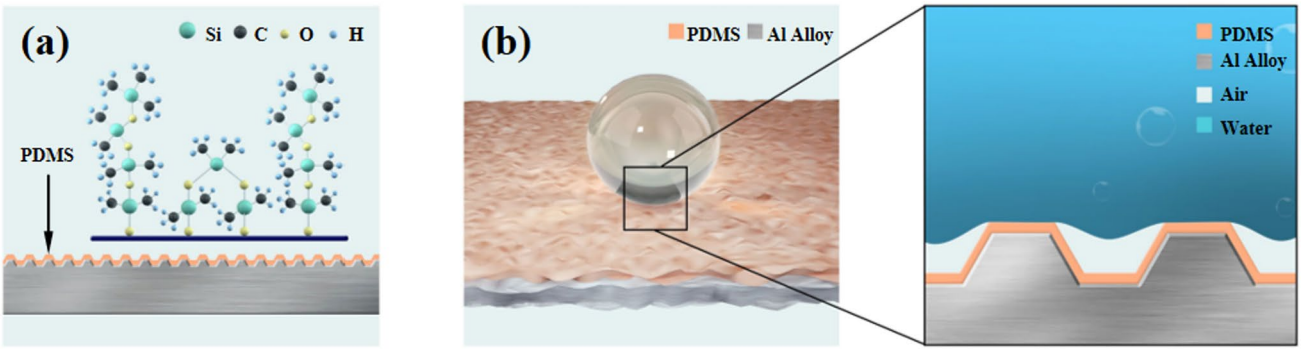


**Fig. 5** The structure of etched surface treated with PDMS and schematic diagram of a water droplet staying on the superhydrophobic surface (**a**) as well as liquid suspension on the structure (**b**)

**Table 2** CA and SA of treated-Al-40 preserved for different period time

| Time (day) | CA (°) | SA (°) |
|---|---|---|
| 0 | 161.1 ± 1.2 | 6.7 ± 0.3 |
| 5 | 161.5 ± 0.9 | 6.9 ± 0.4 |
| 10 | 160.8 ± 0.7 | 7.0 ± 0.9 |
| 15 | 162.2 ± 1.1 | 6.5 ± 0.7 |
| 20 | 161.3 ± 0.5 | 6.8 ± 0.3 |
| 25 | 160.9 ± 1.0 | 7.3 ± 1.0 |
| 30 | 161.2 ± 0.8 | 6.8 ± 0.7 |

The wetting properties of as-prepared superhydrophobic samples after 5 days, 10 days even one month have been tested as shown in Table 2. The CA and SA of treatedtreated-Al-40 sample have barely changed, indicating that as-prepared superhydrophobic surface shows a good wetting stability.

To evaluate the durability of the as-prepared superhydrophobic material, the thermal stability is performed. It can be seen from the Fig. 6, the CA values are changed slightly after freezing or heating from − 20 to 300 °C for treated-Al-40. However, the SA values changes obviously in the temperature below 0 °C and above 240 °C, indicating superhydrophobicity descends gradually. To evaluate stability of surfaces in the aqueous solution, the modified sample was soaked in 3.5 wt% NaCl solution for varying time. After that, CA and SA of treated-Al-40 were measured and plotted in Fig. 7. It is observed that the superhydrophobic property for the sample prepared by chemical etching combining with PDMS modification was still maintained during 12 h of immersion. It is noted that CA slightly decreases with immersion time and its value is found to be 156° after

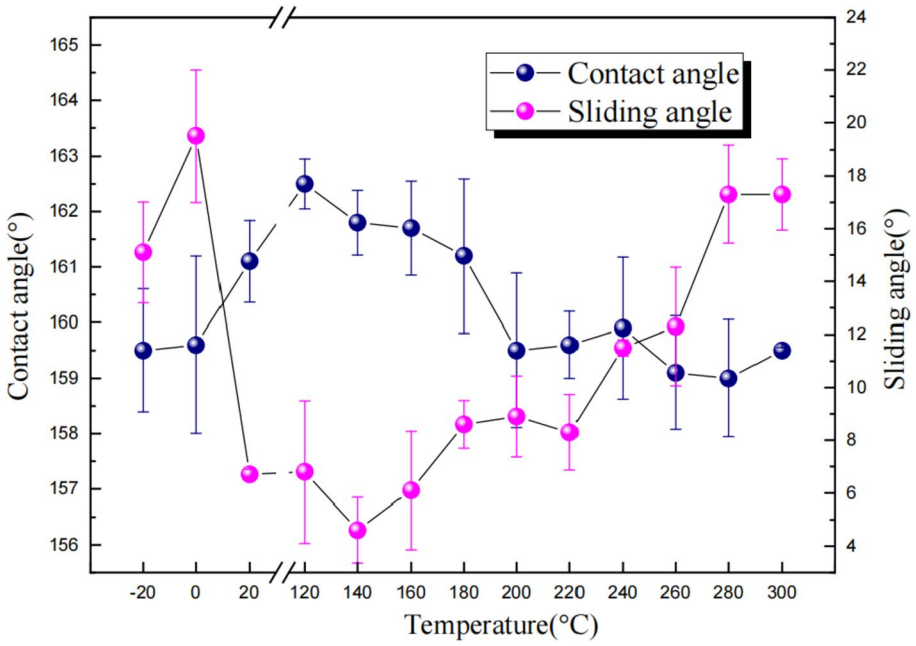


**Fig. 6** CA and SA of treated-Al-40 with heating treatment under different temperature

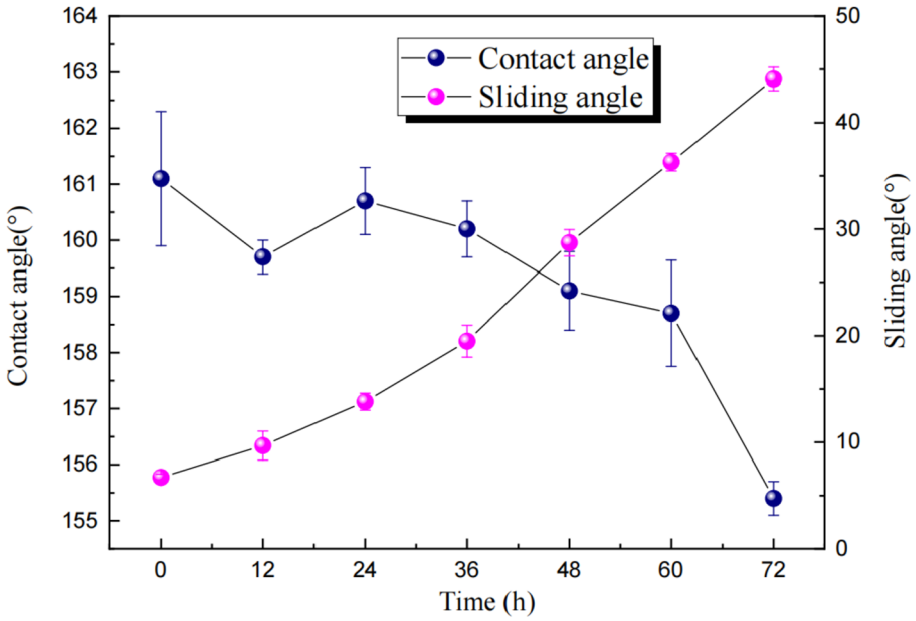


**Fig. 7** CA and SA of treated-Al-40 in the process of soaked in 3.5 wt% NaCl solution

72 h, indicating sample prepared in this work shows a good chemical stability.

### 3.3 Performances of the superhydrophobic surface

Inspired by the outstanding anti-fouling an ability of lotus leaf, a test about self-cleaning behavior of different aluminum alloy surfaces was conducted in Fig. 8. To begin with, a layer of carbon black was well distributed on the surfaces of Al and treated-Al-40, respectively, keeping an angle of approximately 10° from horizontal. Figure 8 demonstrates that when more water droplets dropped onto the surface of treated-Al-40, it could clean up the carbon black along its rolling trace, while this self-cleaning phenomenon could not be observed on the surfaces of other samples. To further verify the self-cleaning property of treated-Al-40, different liquids were poured from a certain height to as-prepared surfaces. As shown in Fig. 9, only a small amount of droplets of dyed water and muddy water stay on superhydrophobic surfaces while original aluminum are covered by water film and contaminated. This phenomenon is consistent with lotus effect, which provides a potential application to outside surfaces beautifully.

Water droplet impacting is an important factor for the practical applications of superhydrophobic surfaces, which has been attracted more and more attentions for the past decades [26, 27]. In this experiment, the dynamic behavior of droplets impacting on the surface of normal aluminum and superhydrophobic aluminum was captured and recorded. Figure 10 shows the snapshots of 20 μL droplets free-falling from 50 mm height to untreated Al and treated-Al-40, respectively. Indoor temperature

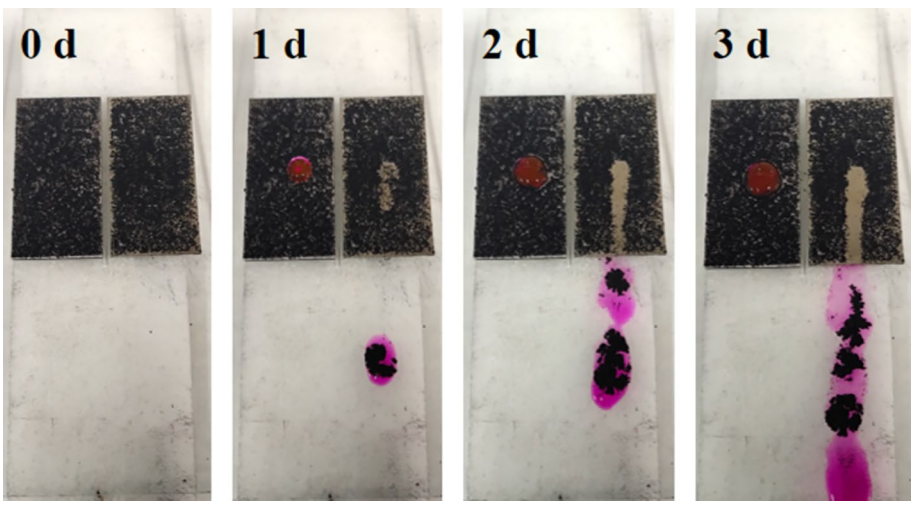


**Fig. 8** The behaviors of water droplets on different surfaces with carbon black (left, Al; right, treated-Al-40); from left to right, the water droplet gradually increased from one drop to three drops

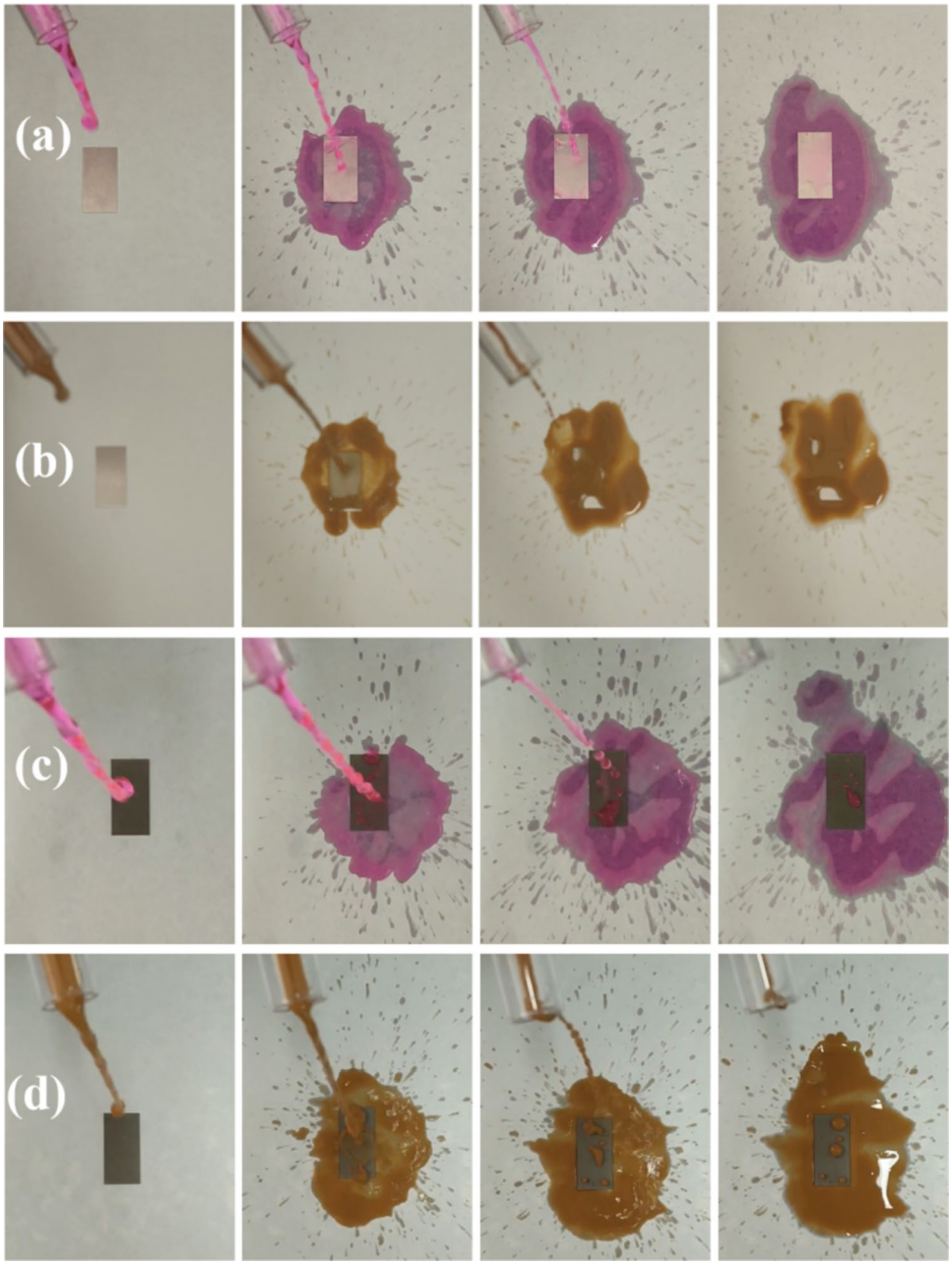


**Fig. 9** The images of dyed water (**a**, **c**) and muddy water (**b**, **d**) poured from a certain height to Al (**a**, **b**) and treated-Al-40 (**c**, **d**)

and humidity remain unchanged. At the beginning of the spreading process, the water droplet is almost like a sphere, which is meant that the geopotential energy is entirely converted into kinetic energy [28]。 It can be seen that from 0 to 4 ms the droplet gradually spreads out, converting the kinetic energy of the droplet into surface energy, and becomes a thick disk that achieves the maximum diameter and the minimum velocity at 4 ms. Different from the original aluminum alloy surface, at the treated-Al-40 surface the liquid droplet shows the spring back behavior. The liquid droplet departs from the modified surface at 20 ms and splits into two drops, which suggests the formation of a solid–air–liquid interface [29]. However, the droplet on the untreated Al surface did not rebound. The dynamic behavior of water droplets shows that the Al surface treated by PDMS has good adhesion resistance and superhydrophobicity.

From Fig. 11, it can be seen that the corrosion potential (Ecorr) of Al is − 1.26 V. Compared to Al, the Ecorr of treated-Al-40 is positively shifted and increased to − 0.58 V. Moreover, the corrosion current density (Icorr) of treated-Al-40 is $1.5 \times 10^{-8}$ A/cm$^2$, and the corrosion current density (Icorr) of treated-Al-40 is decreased to $2.5 \times 10^{-9}$ A/cm$^2$. Generally, the superhydrophobic surface shows a positively shifted Ecorr and a high corrosion resistance [30]. Thus, the anti-corrosion properties of aluminum alloy were greatly

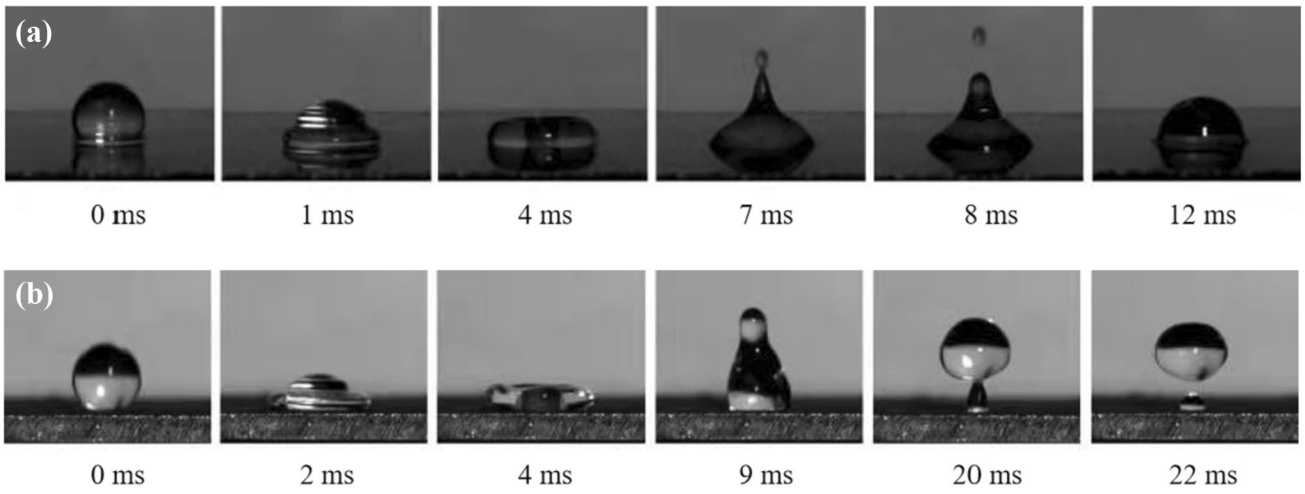


**Fig. 10** The bouncing behaviors of water droplets on Al (**a**) and treated-Al-40 (**b**)

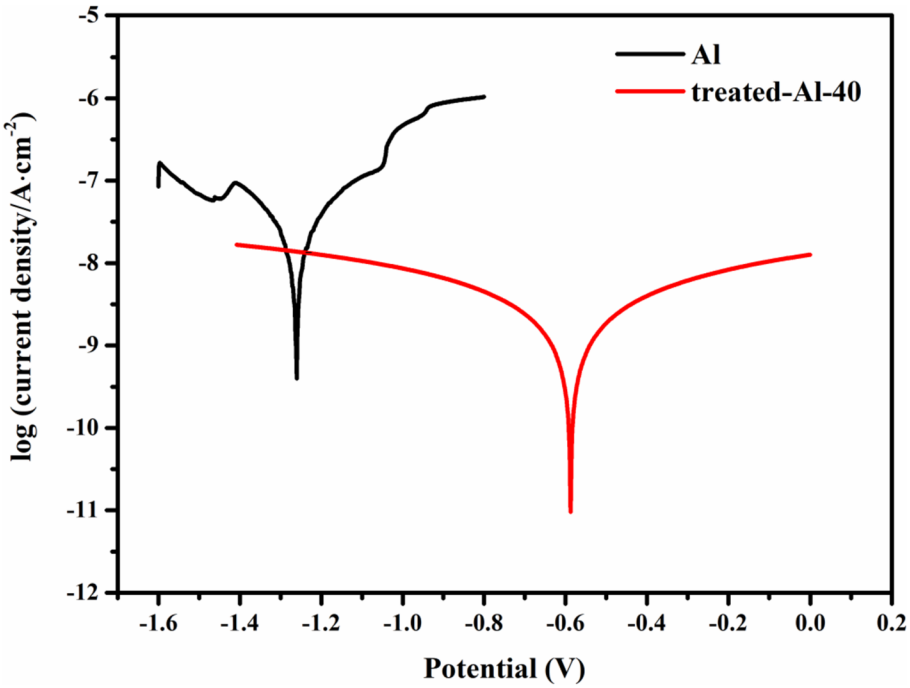


**Fig. 11** Tafel curves of Al and treated-Al-40

enhanced after modification by chemical etching and PDMS coating.

Figure 12 shows the icing accumulation of untreated aluminum alloy and treated-Al-40 at different temperatures of 0 °C, − 5 °C and − 10 °C in the initial state, 30 min, 1 h and 2 h, respectively. As can be seen from these photographs, with the passage of time, more and more water droplets condenses on the surface of aluminum alloy in the low-temperature environment. However, it can be found that the water droplets on the surface of treated-Al-40 are much less than those on the surface of aluminum alloy without treatment, as can be clearly seen from Fig. 12a2, b2, c2. Moreover, as time goes on water droplets on the surface of Al freeze gradually, but the ice area on the surface of treated-Al-40 is much smaller than that on the surface of original aluminum alloy, as can be clearly seen from Fig. 12a4, b4, c4.

To study the freezing characteristics of water droplets on original aluminum alloy surface and treated-Al-40, the freezing process on cold surfaces are observed as shown in Fig. 13. It is obvious that supercooling process of water droplet on original aluminum alloy surface lasts for 0.08 s while that on treated-Al-40 is 0.4 s. In this case,

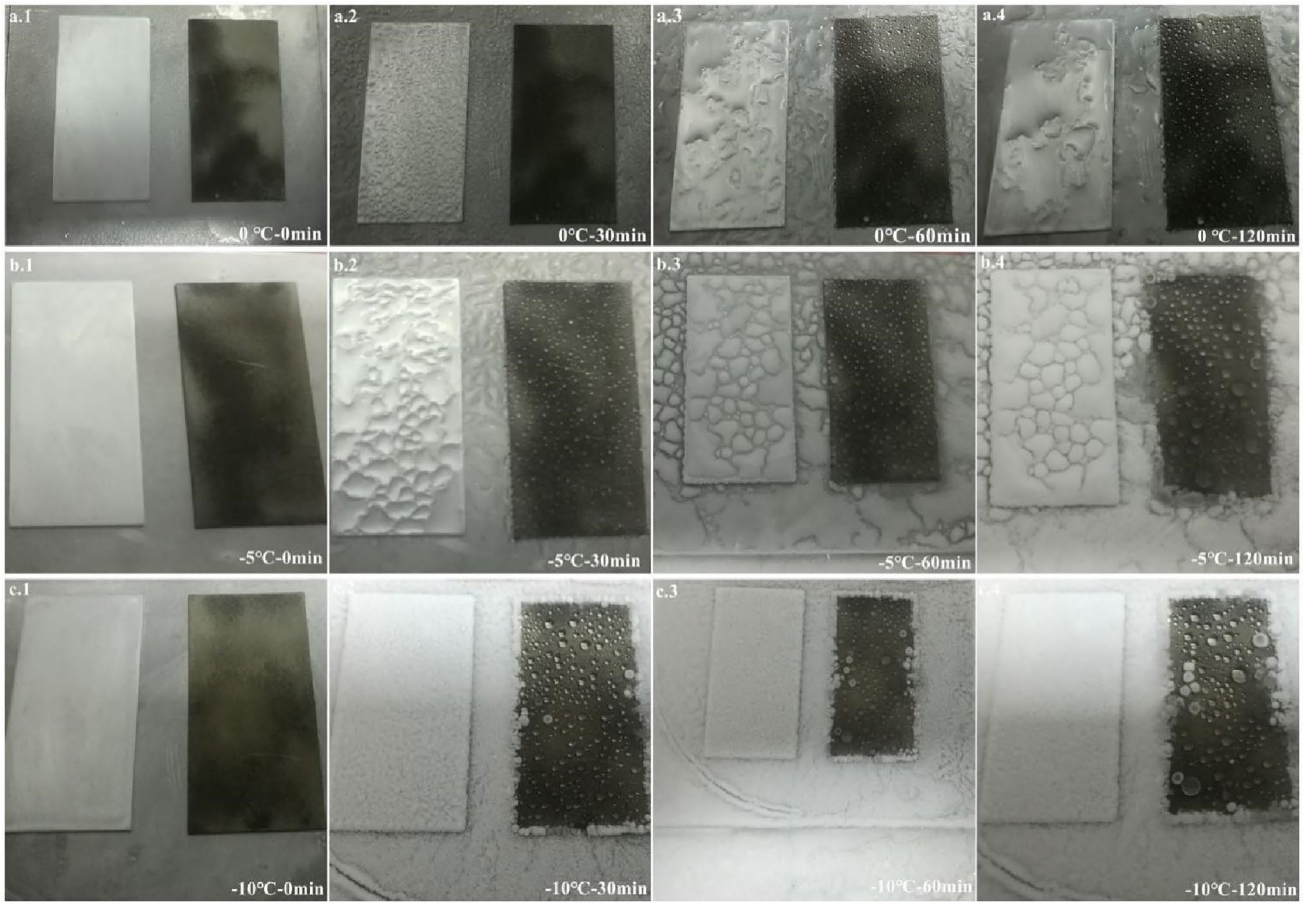


**Fig. 12** Images of ice formation on the surfaces of Al (left) and treated-Al-40 (right) at different temperatures and test time

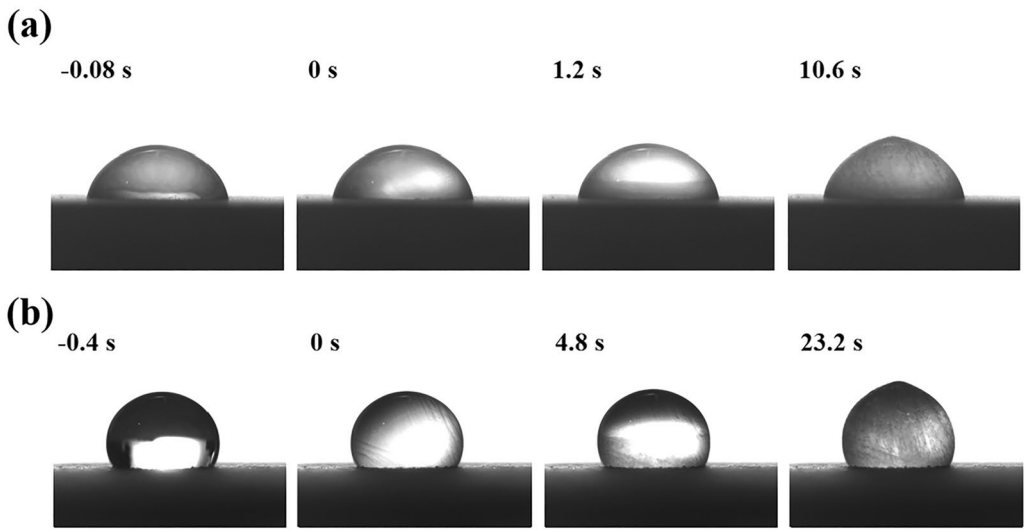


**Fig. 13** Cooling and freezing sequence of water droplet (5 μL) on Al (**a**) and treated-Al-40 (**b**) surface at − 5 °C

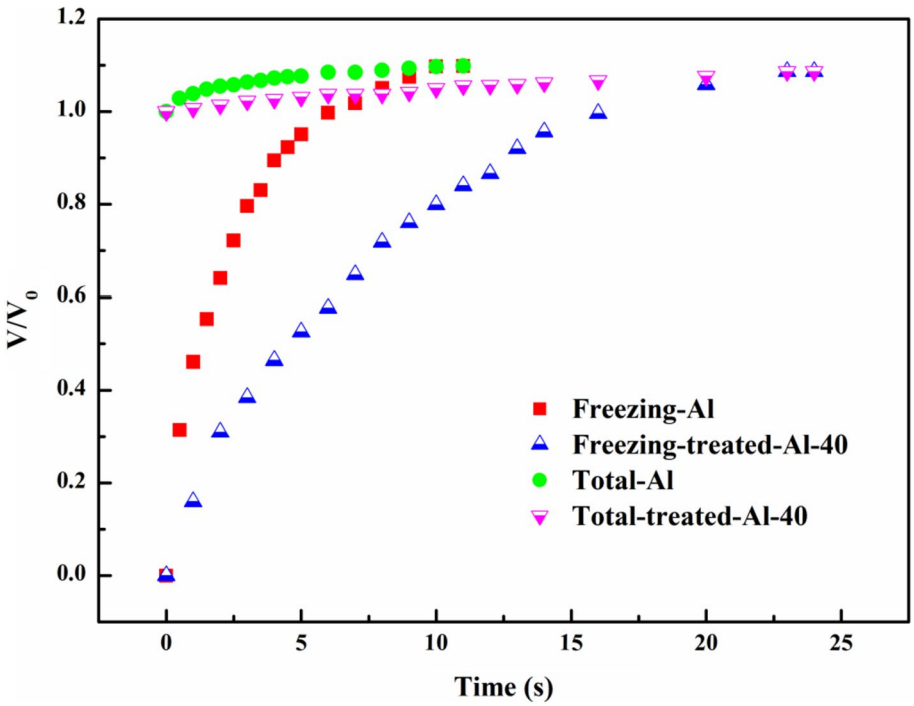


**Fig. 14** Changes in water droplet volume and freezing volume

the freezing of water droplets begins immediately after contacting with cool surface. The ice formation starts near the liquid–solid interface, and freezing front rises from contact surface to the highest point. The freezing time on Al and treated-Al-40 come out to be about 10.6 s and 23.2 s respectively, suggesting that the freezing process of water droplet on superhydrophobic surface takes more than double the time of original aluminum alloy.

The change of the volume of water droplet and frozen ice with time during the droplet freezing process are plotted in Fig. 14. At the beginning, liquid water turned into ice at a very fast rate. Such a rapid phase transition process decreases gradually with time and approaches a constant value at the icing process, Moreover, the volume of water droplets and frozen ice have a relatively flatter trend of evolution compared to Al, providing the anti-icing property of superhydrophobic surface. Since trapped air exists between the water droplet and cold superhydrophobic surface, the process of heat transfer is changed correspondingly thus the crystallization is delayed [31–33]. The equation of heat transfer is expressed as follows:

$$Q = \alpha Sd(T\mathrm{s} - Td), \tag{6}$$

where $Q$ is the net heat gain in unit time; $\alpha$ is the thermal conduction coefficient; $S_d$ is the contact area between droplet and surface; $T_s$ and $T_d$ are the temperatures of surface and water droplet, respectively. For the synthesized superhydrophobic surface, the trapped air takes up a very high percentage, furthermore a smaller liquid–solid contact area causes a slower heat transfer process that explains why a superhydrophobic surface can delay water crystallization.

## 4 Conclusion

Superhydrophobic surfaces have been fabricated on 4037 aluminum alloy plates via a cost-effective processing consisting of chemical etching with $HCl/H_2O_2$, and modifying with petroleum ether containing a low level of PDMS. A water contact angle as 161° and a sliding angle as low as 7° were obtained on the prepared surface. When PDMS to petroleum ether at 0.2 g: 40 mL (treated-Al-40), CA and SA both reach optimal. Hierarchical structure of the superhydrophobic surface are characterized, moreover a possible bonding mechanism of PDMS molecules with aluminum alloy surface during the modification is discussed. Through the test of stability, self-cleaning, droplet dynamic characteristics, corrosion resistance and anti-ice behavior of superhydrophobic surface, it shows that the superhydrophobic surface treated by chemical etching has certain application value.

**Acknowledgements** This work is financially supported by the National Natural Science Foundation of China (U1833202).

## Declarations

**Conflict of interest** There are no conflicts of interest to declare.

## References


1. S.Y. Li, Y. Li, J. Wang, Y.G. Nan, B.H. Ma, Z.L. Liu, J.X. Gu, Chem. Eng. J. **290**, 82 (2016)
2. Y. Zheng, H. Bai, Z. Huang, X. Tian, F.Q. Nie, Y. Zhao, J. Zhai, L. Jiang, Nature **463**, 640–643 (2010)
3. J.W. Sun, H.C. Bi, H.Y. Jia, S. Su, H. Dong, X. Xie, L.T. Sun, J. Clean. Prod. **244**, 118814 (2020)
4. M.P. Yang, W.Q. Liu, L.Y. Liang, C. Jiang, C.H. Liu, Y.K. Xie, H.Y. Shi, F.Y. Zhang, K. Pi, Cellulose **27**, 2847–2857 (2020)
5. G.B. Hwang, A. Patir, K. Page, Y. Lu, E. Allan, I.P. Parkin, Nanoscale **9**, 7588–7594 (2017)
6. M. Ruan, W. Li, B.S. Wang, B.W. Deng, F.M. Ma, Z.L. Yu, Langmuir **29**, 8482–8491 (2013)
7. J. Zhu, X. Hu, Mater. Lett. **190**, 115–118 (2017)
8. D. Choi, J. Yoo, S.M. Park, S.K. Dong, Appl. Surf. Sci. **393**, 449–456 (2017)
9. M. Manca, A. Cannavale, M.L. De, A.S. Aricò, R. Cingolani, G. Gigli, Langmuir **25**, 6357–6362 (2009)
10. A.V. Rao, S.S. Latthe, S.A. Mahadik, C. Kappenstein, Appl. Surf. Sci. **257**, 5772–5776 (2011)
11. T. Hang, A.M. Hu, H.Q. Ling, M. Li, D.L. Mao, Appl. Surf. Sci. **256**, 2400–2404 (2010)
12. J. Li, F. Du, X.L. Liu, Z.H. Jiang, L.Q. Ren, J. Bionic Eng. **8**, 369–374 (2011)
13. H. Wang, D. Dai, X.D. Wu, Appl. Surf. Sci. **254**, 5599–5601 (2008)
14. S.D. Lee, G.H. Hsiue, C.Y. Kao, P.C.T. Chang, Biomaterials **17**, 587–595 (1996)
15. J.H. Park, K.D. Park, Y.H. Bae, Biomaterials **20**, 943–953 (1999)
16. N. Volcker, D. Klee, H. Hocker, S. Langefeld, Mater. Med. **12**, 111–119 (2001)
17. S. Hu, X. Ren, M. Bachmann, C.E. Sims, G.P. Li, N.L. Allbritton, Anal. Chem. **74**, 4117–4123 (2003)
18. J. Roth, V. Albrecht, M. Nitschke, C. Bellmann, F. Simon, S. Zschoche, S. Michel, C. Luhmann, K. Grundke, B. Voit, Langmuir **24**, 12603–12611 (2008)
19. D. Sun, B.B. Li, Z.L. Xu, Korean J. Chem. Eng. **30**, 2059–2067 (2013)
20. G. Slaughter, B. Stevens, BioChip. J. **8**, 28–34 (2014)
21. R.J. Higgins, W.E. Rhine, M.J. Cima, H.K. Bowen, E.R. William, J. Am. Ceram. Soc. **77**, 2243–2253 (1994)
22. B. Dhananjay, K.M. Chantal, J. Microelectron, Microelectron. Eng. **83**, 1277–1279 (2006)
23. K. Seo, M. Kim, S. Seok, D.H. Kim, Colloid Surf. A. **492**, 110–118 (2016)
24. W.L. Qiu, D. Xu, B. Liu, S. Lie, Q.P. Guo, RSC Adv. **5**, 71329–71335 (2015)
25. A.B.D. Cassie, S. Baxter, Trans. Faraday Soc. **40**, 546–551 (1994)
26. Y.C. Yong, B. Bhushan, Langmuir **25**, 9208 (2009)
27. K.X. Meng, W.L. Fan, H. Wang, Appl. Therm. Eng. **148**, 316 (2019)
28. B. Ding, H. Wang, X. Zhu, R. Chen, Q. Liao, Int. J. Heat Mass Tran. **124**, 1025 (2008)
29. Y.C. Jung, B. Bhushan, Langmuir **24**, 6262 (2008)
30. X.W. Li, L. Zhang, T. Shi, C.W. Zhang, L.C. Zhang, Mater. Corros. **70**, 558–565 (2019)
31. T.B. Nguyen, S. Park, H. Lim, Appl. Surf. Sci. **435**, 585–591 (2018)
32. S.B. Subramanyam, V. Kondrashov, J. Rühe, K.K. Varanasi, A.C.S. Appl, Mater. Inter. **8**, 12583–12587 (2016)
33. A. Davis, Y.H. Yong, A. Steele, I.S. Bayer, E. Loth, Appl. Mater. Inter. **6**, 9272–9279 (2014)